

Article

Exploring the Dynamics of Dark and Singular Solitons in Optical Fibers Using Extended Rational Sinh–Cosh and Sine–Cosine Methods

Annamalai Muniyappan ¹, Kannan Manikandan ^{1,2,*} , Akbota Saparbekova ³ and Nurzhan Serikbayev ^{2,4,*}

¹ Center for Computational Modeling, Chennai Institute of Technology, Chennai 600 069, Tamilnadu, India; muniyappana@citchennai.net

² Department of General and Theoretical Physics, L. N. Gumilyov Eurasian National University, 010008 Astana, Kazakhstan

³ Department of Mathematics, Physics and Computer Science, Sh. Ualikhanov Kokshetau University, 020000 Kokshetau, Kazakhstan; asaparbekova@shokan.edu.kz

⁴ Laboratory for Theoretical Cosmology, International Centre of Gravity and Cosmos, Tomsk State University of Control Systems and Radio Electronics (TUSUR), 634050 Tomsk, Russia

* Correspondence: manikandank@citchennai.net (K.M.); serikbayev_ns@enu.kz (N.S.)

Abstract: This investigation focuses on the construction of novel dark and singular soliton solutions for the Hirota equation, which models the propagation of ultrashort light pulses in optical fibers. Initially, we employ a wave variable transformation to convert the physical model into ordinary differential equations. Utilizing extended rational sinh–cosh and sine–cosine techniques, we derive an abundant soliton solution for the transformed system. By plugging these explicit solutions back into the wave transformation, we obtain dark and singular soliton solutions for the Hirota equation. The dynamic evolution of dark soliton profiles is then demonstrated, with a focus on varying physically significant parameters such as wave frequency, strength of third-order dispersion, and wave number. Furthermore, a comprehensive analysis is examined to elucidate how the dark and singular soliton profiles undergo deformation in the background influenced by these arbitrary parameters. The findings presented in this study offer valuable insights that could potentially guide experimental manipulation of dark solitons in optical fibers.

Keywords: optical soliton; Hirota equation; nonlinear Schrödinger equation; optical fibers; wave transformation



Citation: Muniyappan, A.; Manikandan, K.; Saparbekova, A.; Serikbayev, N. Exploring the Dynamics of Dark and Singular Solitons in Optical Fibers Using Extended Rational Sinh–Cosh and Sine–Cosine Methods. *Symmetry* **2024**, *16*, 561. <https://doi.org/10.3390/sym16050561>

Academic Editor: Sergei D. Odintsov

Received: 3 April 2024

Revised: 24 April 2024

Accepted: 26 April 2024

Published: 4 May 2024



Copyright: © 2024 by the authors. Licensee MDPI, Basel, Switzerland. This article is an open access article distributed under the terms and conditions of the Creative Commons Attribution (CC BY) license (<https://creativecommons.org/licenses/by/4.0/>).

1. Introduction

Optical fibers can give rise to envelope solitons when the self-phase modulation precisely counteracts the group velocity dispersion. Solitons, characterized as shape-preserving wave packets, can propagate through nonlinear dispersive media without undergoing spreading. The investigation of these particle-like excitations has attracted considerable interest owing to their promising applications in high-capacity fiber optical communications and all-optical switching. They are particularly regarded as strong candidates for enabling high-bandwidth, high-speed, and long-distance optical communication systems. This is attributed to their ability to maintain a stable shape in the time domain throughout extended optical fiber transmissions, highlighting their potential robustness and efficacy in practical communication scenarios [1–5].

In recent years, the study of dark soliton propagation in nonlinear media has garnered considerable attention through both theoretical and experimental investigations. This localized wave has been discerned across various nonlinear systems, encompassing Bose–Einstein condensates, nonlocal media characterized by competing nonlinearities, photovoltaic photorefractive materials, nematic liquid crystals, and optical fibers. Their manifestation in such diverse settings underscores their fundamental nature and their

relevance in elucidating nonlinear phenomena across different scientific domains [6–9]. In the context of optical fibers, the inception of dark solitons under normal dispersion conditions was first anticipated by Hasegawa and Tappert [10], as well as by Zakharov and Shabat [11]. Dark solitons exhibit intriguing properties, such as heightened resilience to perturbations compared to their bright counterparts, including those arising from loss and amplified spontaneous emission noise. Experimental evidence for their existence was provided by Emplit et al. [12], who characterized them as nontrivial phase-profiled localized intensity dips on a continuous wave background. Subsequently, dark soliton generation in fiber lasers [8,13–16] has been observed experimentally in fiber lasers, and the formation mechanism is currently being studied, along with the development of systems to measure the narrow dark pulses as they form in the laser. In an interesting experimental demonstration, Zhang et al. [8] demonstrated the emission of dark localized pulses from an erbium-doped fiber laser with all-normal dispersion. According to their research, fiber lasers can emit single or multiple dark pulses under appropriate operating conditions. Furthermore, Tang et al. [17] showcased the presence of dark solitons within all-normal-dispersion fiber lasers, emphasizing their intrinsic formation. Remarkably, these dark solitons can be generated without a threshold value in the input-pulse power. The practical utility of these phenomena extends to various applications, including optical logic devices, all-optical switches, and waveguide optics.

In the realm of picosecond dynamics, the behavior of solitons in single-mode fibers is classically described by the cubic nonlinear Schrödinger (NLS) equation, a scalar field model often derived using the slowly-varying envelope approximation. However, when injecting ultrashort light pulses, with durations less than 100 fs, it becomes imperative to account for higher-order nonlinear properties such as self-steepening and delayed nonlinear response [7,18,19]. These effects are crucial as they profoundly impact the nonlinear optical system. In addition to this, the introduction of extremely short pulses, typically around 50 fs in width, into optical wave-guiding media accentuates the significance of third-order dispersion, demanding meticulous attention. This inclusion of higher-order dispersion not only induces pulse asymmetry but also precipitates radiation phenomena. To comprehensively capture these complex physical phenomena, the NLS equation is extended to incorporate additional higher-order phenomena [20–23]. This refined model, denoted as the higher-order NLS equation, enables a more precise portrayal of wave dynamics in practical materials, particularly concerning light propagation in optical fibers. The imperative for the higher-order NLS equation stems from the intrinsic necessity to accommodate the impacts of higher-order nonlinear and dispersive phenomena inherent in optical fibers. While incorporating these significant effects complicates both theoretical analyses and experimental observations of optical solitons, the optical solitons generated under such conditions hold promise for unveiling novel nonlinear phenomena and offering deeper insights into basic nonlinear mechanisms [14,24–27].

Inspired by advancements in higher-order NLS equations, we delve into the exploration of dark and singular (bright) soliton solutions by considering the third-order NLS equation, also known as the Hirota equation. Through this investigation, we aim to analyze the notable characteristics associated with these soliton solutions by adjusting the system parameters. Exploring solitary wave solutions for nonlinear equations is pivotal in unraveling various nonlinear physical phenomena [28–35]. Nonlinear wave phenomena manifest across a spectrum of engineering and scientific domains, encompassing fluid dynamics, plasma physics, optics, biology, condensed matter physics, and beyond [1,9]. To understand the nonlinear wave phenomena and construct the solitary wave solutions in the nonlinear partial differential equations, endeavors have been attempted to utilize the various techniques, one may refer [36–41]. In particular, in ref. [42], the rational sine-cosine method and rational sinh-cosh method have been extended to construct new exact solutions of the nonlinear perturbed Schrödinger equation with Kerr law nonlinearity. This approach yields a wealth of new exact traveling wave solutions, expressed in various forms including hyperbolic functions, trigonometric functions, and complex functions [43–45]. In

this work, we also utilize the extended rational sinh–cosh method and extended rational Sin–Cosine method, renowned for their simplicity and effectiveness, to construct dark and singular soliton solutions for the Hirota equation under consideration. Moreover, we analyze the dynamic properties of dark solitons by systematically varying parameters such as the strength of the third-order dispersion, wave speed, and wave frequency. Our findings unveil intriguing dynamics, including variations in the intensity of dark soliton profiles, enhancements, and suppression of amplitudes, as well as alterations in their orientations.

The motivation of this work is to investigate the impact of physical parameter strengths on the dynamics of solitons and to bring out their salient features through explicit solutions and graphical demonstrations. To achieve these, we design the manuscript in the following manner: In Section 2, we recall the solution techniques such as extended rational sinh–cosh and sine–cosine methods. In Section 3, we take into account the Hirota equation for deriving the explicit soliton solutions and explore the various dynamical behaviors by changing physically significant parameters. The final section, Section 4, contains a brief discussion of the conclusions derived from this work.

2. Solution Technique

We outline the first stage of newly extended rational methods aimed at identifying exact solutions for partial differential equations, as follows:

$$F\left(g, \frac{\partial g}{\partial t}, \frac{\partial g}{\partial x}, \frac{\partial^2 g}{\partial x^2}, \dots\right) = 0. \quad (1)$$

In Equation (1), the variable $g = g(x, t)$ represents an unspecified function, and F denotes a polynomial in g as well as its diverse partial derivatives. This equation encapsulates a relationship where the function g and its derivatives, as manipulated within the polynomial F , collectively contribute to the overall solution. Let us consider $g(x, t)$ as a traveling wave solution of Equation (1). By substituting the following transformation:

$$\psi(x, t) = g(\eta), \quad \eta = x - vt, \quad (2)$$

into Equation (1), it can be transformed into an ordinary differential equation of the form $P(g, g', g'', g''', \dots)$, where prime indicates $\frac{\partial}{\partial \eta}$.

2.1. Extended Rational Sinh–Cosh Approach

Step 1: Let us consider Equation (2) and propose a solution in the form as described in [42–44]

$$g(\eta) = \frac{p_0 \sinh(\mu\eta)}{p_2 + p_1 \cosh(\mu\eta)}, \quad \cosh(\mu\eta) \neq -\frac{p_2}{p_1}, \quad (3)$$

or

$$g(\eta) = \frac{p_0 \cosh(\mu\eta)}{p_2 + p_1 \sinh(\mu\eta)}, \quad \sinh(\mu\eta) \neq -\frac{p_2}{p_1}, \quad (4)$$

where p_0 , p_1 , and p_2 are parameters yet to be determined, and μ represents the wave number.

Step 2: To determine the unknown constants, we insert Equation (3) or Equation (4) into Equation (1). We gather expressions with the same power of $\cosh(\mu\eta)^m$ or $\sinh(\mu\eta)^m$ and equate the coefficients of these terms to zero. This process yields a set of algebraic equations, the solution of which enables us to determine the values of the unknown parameters.

Step 3: Once the constants p_0 , p_1 , p_2 , and μ are, we proceed to derive the solution of Equation (1) by substituting these determined values into either Equation (3) or Equation (4). This step completes the process, providing us with the solution of the given equation.

2.2. Extended Rational Sin–Cosine Approach

Step 1: Let us commence with the assumption that Equation (2) admits a solution to the following form [42–44]:

$$g(\eta) = \frac{p_0 \sin(\mu\eta)}{p_2 + p_1 \cos(\mu\eta)}, \quad \cos(\mu\eta) \neq -\frac{p_2}{p_1}, \quad (5)$$

or

$$g(\eta) = \frac{p_0 \cos(\mu\eta)}{p_2 + p_1 \sin(\mu\eta)}, \quad \sin(\mu\eta) \neq -\frac{p_2}{p_1}, \quad (6)$$

where p_0 , p_1 , and p_2 are parameters to be determined.

Step 2: In order to determine the unknown constants, we substitute Equation (5) or Equation (6) into Equation (1). By consolidating terms with the same powers of $\cos(\mu\eta)^m$ or $\sin(\mu\eta)^m$ and setting the coefficients of these terms to zero, we derive a system of algebraic equations. The solutions to these equations unveil the values of the unknown parameters.

Step 3: With the constants p_0 , p_1 , p_2 , c , and μ discerned, we proceed to uncover the solution of Equation (1) by substituting these values into Equation (5) or Equation (6). This final step completes the process, furnishing us with the solution to the given equation.

3. Third-Order NLS Equation and Dark/Singular Soliton Solutions

Dark solitons, observed experimentally in various physically significant systems, often exhibit intricate dynamics, particularly when their formation results from a delicate balance among higher-order effects. Although features like power for dark soliton formation, pulse width, and soliton velocity can be experimentally measured, the rapid changes in these characteristics and the complex dynamics of dark pulses pose challenges for a comprehensive understanding based solely on experimentation. To delve deeper into these phenomena, a theoretical description of the propagation features of these localized nonlinear structures becomes crucial. This necessitates a detailed analytical analysis founded on models featuring a more general form of the intensity-dependent refractive index, especially when studying soliton behavior in non-Kerr materials. Such theoretical exploration is essential for unraveling the nuanced behavior of dark solitons and gaining insights into various associated phenomena [14,24–27]. Motivated by these developments, in this work, we consider the higher-order NLS equation, namely third-order NLS or the Hirota equation [22–24] for investigating the dynamical features of dark soliton solutions, as follows:

$$i\psi_t + \alpha_2 (\psi_{xx} + 2|\psi|^2\psi) + i\alpha_3 (\psi_{xxx} + 6|\psi|^2\psi_x) = 0. \quad (7)$$

In Equation (7), the complex wave envelope is represented by the function $\psi(x, t)$, where α_2 and α_3 serve as arbitrary parameters. The subscripts t and x signify partial derivatives concerning temporal and spatial variables, respectively. The Hirota Equation (7) provides a framework for describing the propagation of ultrashort light pulses in optical fibers [25,26]. It is intriguing to observe that the Hirota Equation (7) exhibits a composite nature, comprising elements from both the NLS equation and the complex variant of the modified Korteweg–de Vries equation. Specifically, when considering the parameter values $\alpha_2 = 1$ and $\alpha_3 = 0$, the Hirota equation reduces to the NLS equation, i.e., $i\psi_t + \psi_{xx} + 2|\psi|^2\psi = 0$. Conversely, with $\alpha_2 = 0$ and $\alpha_3 = 1$, the Hirota equation corresponds to the complex version of the modified Korteweg–de Vries equation, i.e., $\psi_t + \psi_{xxx} + 6|\psi|^2\psi_x = 0$. This amalgamation of equations reflects the intricate interplay between different physical phenomena, offering deeper insights into the dynamics of wave propagation in various systems. In the past two decades, extensive research efforts have been directed toward the construction and analysis of localized solutions in the Hirota equation [22,23,26,46,47]. For instance, periodic solutions have been derived by Crabb et al. [22], while Sinthuja et al. [23] focused on constructing rogue wave solutions over the double periodic wave backgrounds for the

Hirota Equation (7). Ankie et al. [46] tackled the problem by constructing a hierarchy of rational solutions using a modified Darboux transformation technique. In another study by Zhang et al. [26], dark soliton solutions of the de-focusing Hirota equation were investigated via the binary Darboux transformation technique. Additionally, Shi et al. [47] explored higher-order rogue waves and interactions between solitons and rogue waves using the long wave limit in multi-soliton scenarios. Furthermore, diverse methodologies have been applied to produce multi-solitons, rogue waves, and breather solutions within the framework of the Hirota equation [20,21,26,48]. Inspired by these advancements, our work aims to contribute to this field by employing extended rational sinh–cosh and sine–cosine methods to derive new dark and singular soliton solutions for the Hirota equation.

To explore the solitary wave solutions of the Hirota Equation (7), we assume the wave transformation as follows:

$$\psi(x, t) = g(\eta)e^{i(kx-ct)}, \quad \eta = x - vt, \quad (8)$$

where k , v , and c are constants to be determined later. Upon substituting this wave solution in Equation (7), we collect the real and imaginary parts of the expressions given by the following:

$$g''(\eta) + 2g^3(\eta) + r_1g(\eta) = 0, \quad (9)$$

$$g'''(\eta) + 6g^2(\eta)g'(\eta) - r_2g'(\eta) = 0, \quad (10)$$

where $r_1 = \frac{c+k^2(-\alpha_2+k\alpha_3)}{(\alpha_2-3k\alpha_3)}$, and $r_2 = \frac{v-2k\alpha_2+3k^2\alpha_3}{\alpha_3}$. In the following subsections, we construct solitary wave solutions for a class of Equations (9) and (10). Rigorously speaking, until we can demonstrate their elastic scattering, the solutions should be referred to as “solitary waves”. Nevertheless, given our focus on integrable soliton equations, these solitary wave solutions are anticipated to indeed evolve into solitons eventually. For the sake of simplicity, we consistently label them as solitons throughout our discussion.

3.1. The Implementation of the Extended Rational Sinh–Cosh Technique

To begin with, we attempt to construct a solitary wave solution for the Hirota Equation (7). For this purpose, we choose the following form of solutions for Equations (9) and (10) as follows:

$$g(\eta) = \frac{p_0 \sinh(\mu\eta)}{p_2 + p_1 \cosh(\mu\eta)}, \quad (11)$$

where p_0 , p_1 and p_2 are already mentioned. Plugging Equation (11) into Equations (9) and (10), we congregate the coefficients of $\cosh(\mu\eta)$, as follows:

$$\begin{aligned} \cosh^2(\mu\eta) : 2p_1^2r_1 + 4p_0^2 &= 0, \\ \cosh^1(\mu\eta) : 4p_1p_2r_1 - 2\mu^2p_1p_2 &= 0, \\ \cosh^0(\mu\eta) : -4\mu^2p_1^2 + 2\mu^2p_2^2 + 2p_2^2r_1 - 4p_0^2 &= 0, \end{aligned} \quad (12a)$$

&

$$\begin{aligned} \cosh^3(\mu\eta) : p_1^2(\mu^2 - r_2) + 6p_0^2 &= 0, \\ \cosh^2(\mu\eta) : p_1^2(r_2 - 4\mu^2) + 2p_2^2(2\mu^2 + r_2) - 6p_0^2 &= 0, \\ \cosh^1(\mu\eta) : 2p_1^2(2\mu^2 + r_2) + p_2^2(r_2 - \mu^2) + 6p_0^2 &= 0, \\ \cosh^0(\mu\eta) : 6\mu^2p_1^2 + p_2^2(r_2 - 4\mu^2) + 6p_0^2 &= 0. \end{aligned} \quad (12b)$$

By solving these algebraic Equation (12), the different sets of values p_0 , p_1 , p_2 , and μ are obtained.

Set 1:

$$\begin{aligned} p_0 &= \pm \frac{p_1 \sqrt{3\alpha_3 k^2 - 2\alpha_2 k + \nu}}{\sqrt{2\alpha_3}}, \quad \mu = -\frac{\sqrt{2} \sqrt{-3\alpha_3 k^2 + 2\alpha_2 k - \nu}}{\sqrt{\alpha_3}}, \\ p_2 &= p_1, \quad c = \frac{8\alpha_3^2 k^3 - 8\alpha_2 \alpha_3 k^2 + 2\alpha_2^2 k + 3\alpha_3 k \nu - \alpha_2 \nu}{\alpha_3}. \end{aligned} \quad (13)$$

Substituting these values (13) into (8) along with (11), we obtain the following dark soliton solution:

$$\psi(x, t) = \pm \left(\frac{\frac{p_1 \sqrt{3\alpha_3 k^2 - 2\alpha_2 k + \nu}}{\sqrt{2\alpha_3}} \sinh\left(-\frac{\sqrt{2} \sqrt{-3\alpha_3 k^2 + 2\alpha_2 k - \nu}}{\sqrt{\alpha_3}}(x - \nu t)\right)}{p_2 + p_1 \cosh\left(-\frac{\sqrt{2} \sqrt{-3\alpha_3 k^2 + 2\alpha_2 k - \nu}}{\sqrt{\alpha_3}}(x - \nu t)\right)} \right) \exp(i(kx - ct)). \quad (14)$$

Set 2:

$$\begin{aligned} p_0 &= \pm \frac{p_1 \sqrt{3\alpha_3 k^2 - 2\alpha_2 k + \nu}}{\sqrt{2\alpha_3}}, \quad \mu = \frac{\sqrt{2} \sqrt{-3\alpha_3 k^2 + 2\alpha_2 k - \nu}}{\sqrt{\alpha_3}}, \\ p_2 &= p_1, \quad c = \frac{8\alpha_3^2 k^3 - 8\alpha_2 \alpha_3 k^2 + 2\alpha_2^2 k + 3\alpha_3 k \nu - \alpha_2 \nu}{\alpha_3}. \end{aligned} \quad (15)$$

Inserting the above expressions in (8) with (11), we obtain the following:

$$\psi(x, t) = \pm \left(\frac{\frac{p_1 \sqrt{3\alpha_3 k^2 - 2\alpha_2 k + \nu}}{\sqrt{2\alpha_3}} \sinh\left(\frac{\sqrt{2} \sqrt{-3\alpha_3 k^2 + 2\alpha_2 k - \nu}}{\sqrt{\alpha_3}}(x - \nu t)\right)}{p_2 + p_1 \cosh\left(\frac{\sqrt{2} \sqrt{-3\alpha_3 k^2 + 2\alpha_2 k - \nu}}{\sqrt{\alpha_3}}(x - \nu t)\right)} \right) \exp(i(kx - ct)). \quad (16)$$

Set 3:

$$\begin{aligned} p_0 &= \pm \frac{p_1 \sqrt{3\alpha_3 k^2 - 2\alpha_2 k + \nu}}{\sqrt{2\alpha_3}}, \quad \mu = -\frac{\sqrt{-3\alpha_3 k^2 + 2\alpha_2 k - \nu}}{\sqrt{2\alpha_3}}, \\ p_2 &= 0, \quad c = \frac{8\alpha_3^2 k^3 - 8\alpha_2 \alpha_3 k^2 + 2\alpha_2^2 k + 3\alpha_3 k \nu - \alpha_2 \nu}{\alpha_3}. \end{aligned} \quad (17)$$

The corresponding solitary wave solution is given by the following:

$$\psi(x, t) = \pm \frac{\sqrt{3\alpha_3 k^2 - 2\alpha_2 k + \nu}}{\sqrt{2\alpha_3}} \tanh\left(-\frac{\sqrt{-3\alpha_3 k^2 + 2\alpha_2 k - \nu}}{\sqrt{2\alpha_3}}(x - \nu t)\right) \exp(i(kx - ct)). \quad (18)$$

Set 4:

$$\begin{aligned} p_0 &= \pm \frac{p_1 \sqrt{3\alpha_3 k^2 - 2\alpha_2 k + \nu}}{\sqrt{2\alpha_3}}, \quad \mu = \frac{\sqrt{-3\alpha_3 k^2 + 2\alpha_2 k - \nu}}{\sqrt{2\alpha_3}}, \\ p_2 &= 0, \quad c = \frac{8\alpha_3^2 k^3 - 8\alpha_2 \alpha_3 k^2 + 2\alpha_2^2 k + 3\alpha_3 k \nu - \alpha_2 \nu}{\alpha_3}. \end{aligned} \quad (19)$$

Plugging the above expressions (19) into (8) with (11), we find the following:

$$\psi(x, t) = \pm \frac{\sqrt{3\alpha_3 k^2 - 2\alpha_2 k + \nu}}{\sqrt{2\alpha_3}} \tanh\left(\frac{\sqrt{-3\alpha_3 k^2 + 2\alpha_2 k - \nu}}{\sqrt{2\alpha_3}}(x - vt)\right) \exp(i(kx - ct)). \quad (20)$$

Figure 1 illustrates the qualitative nature of the intensity profile of a dark soliton, utilizing the solution (14) for the considered Hirota Equation (7). Employing parameters $p_1 = 1$, $\nu = 0.01$, $k = 0.25$, $\alpha_2 = 1$, and $\alpha_3 = 0.05$, we present the intensity profile of the dark soliton in Figure 1a, revealing its fundamental features. Upon modifying the value of α_3 to 0.2, the intensity profile reduces, and its width slightly increases, as depicted in Figure 1b. Additionally, there is a noticeable decrease in intensity. Subsequently, with an increase in the value of ν to 0.25, Figure 1c demonstrates a change in the orientation of the dark soliton profile, accompanied by a decrease in amplitude. Further adjustments in the value of k to 0.75 lead to an increase in the amplitude of the dark soliton profile, along with a more compressed width, as illustrated in Figure 1d.

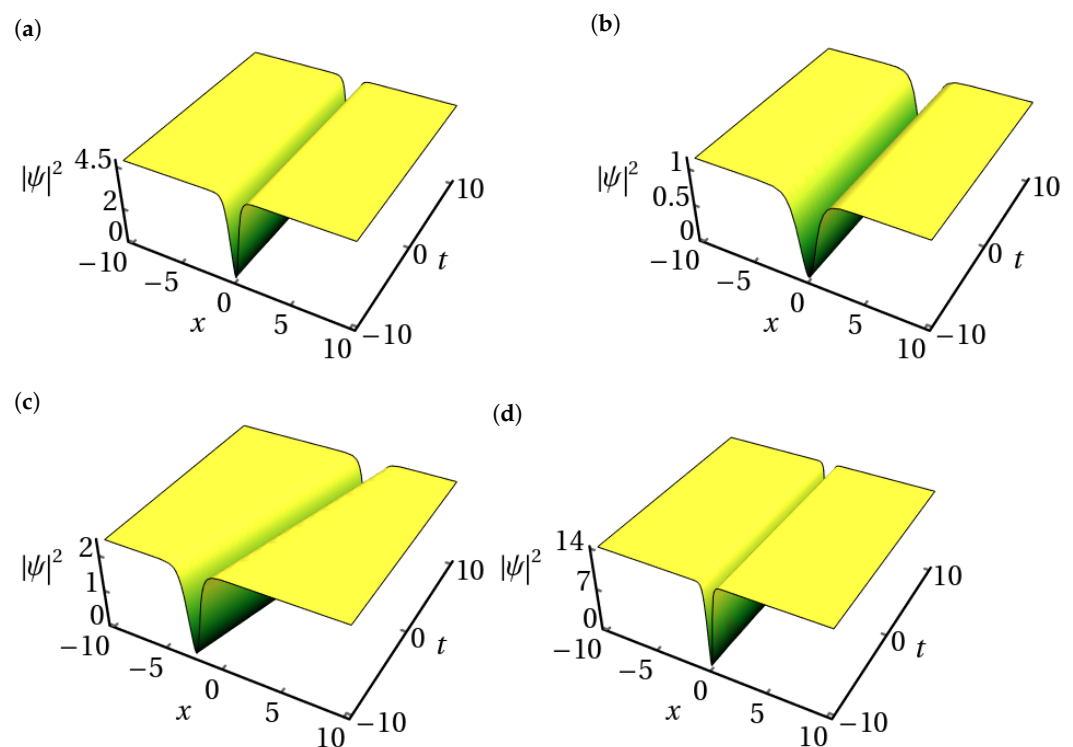


Figure 1. Intensity of dark soliton profiles for the third-order NLS Equation (7) using the solution (14). The parameters are (a) $p_1 = 1$, $\nu = 0.01$, $k = 0.25$, $\alpha_2 = 1$, $\alpha_3 = 0.05$; (b) $\alpha_3 = 0.2$; (c) $\nu = 0.25$; (d) $k = 0.75$. In (b–d), we vary the specified parameters while maintaining all other parameters at the same values as in (a).

To gain a comprehensive insight, we plotted the soliton's amplitude against x at $t = 0.01$, while manipulating various parameters, such as α_3 , ν , and k . These results are depicted in Figure 2. In Figure 2a, we observe different profiles resulting from varying α_3 . Specifically, when α_3 takes values of 0.05, 0.1, and 0.85, the amplitude of the dark soliton profile diminishes, and its width expands noticeably. Moving to Figure 2b, we witness a nuanced behavior as the parameter ν changes. Initially, as ν increases from 0.1 to 0.4, the amplitude of the dark soliton profile decreases while its width expands. Subsequently, selecting $\nu = 0.6$ transforms the dark soliton profile into a periodic form with heightened amplitude. Furthermore, in Figure 2c, we explore the impact of the wave number k with values of 0.1, 0.5, and 1.25. Here, we observe a consistent trend: as k varies, the amplitude

of the dark soliton diminishes, and its width broadens. These findings, as illustrated in Figure 2, provide valuable insights into the behavior of solitons under parameter variations.

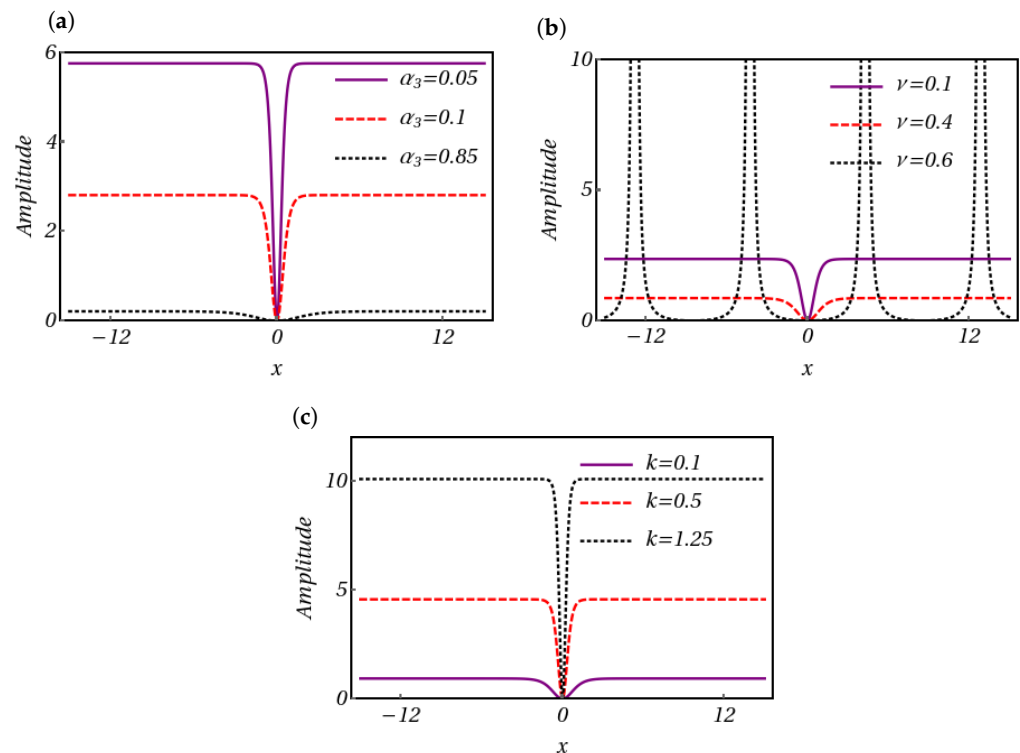


Figure 2. The magnitude variation in the amplitude of dark soliton due to the influence of (a) α_3 , (b) ν , and (c) k at $t = 0.01$. The other parameters are the same in Figure 1a.

In Figures 1 and 2, we present the formation and explore the intriguing features of dark solitons in our considered physical system (7). In the context of optics, these solitons emerge from the intricate interplay among nonlinear effects, dispersion, and attenuation [2,3,49]. The temporal evolution of the intensity profile, as depicted in Figure 1a, unveils the intricate journey of the optical pulse through the fiber. Initially, dispersion effects may induce broadening and distortion of the pulse. However, as it traverses, nonlinear effects stimulate the emergence of the dark soliton, preserving its shape and velocity over considerable distances despite challenges posed by dispersion and attenuation. Furthermore, our investigation reveals variations in the width, orientation, and amplitude of dark solitons by finely tuning the parameters present in their solutions. This fine-tuning is facilitated by leveraging the nonlinear dependence of the refractive index on intensity, offering insights into the versatile behavior of dark solitons. These meticulous investigations not only enable precise measurements of the temporal and spectral properties of optical pulses but also facilitate the detection and study of dark solitons and their propagation dynamics [50,51]. Moreover, the theoretical insights presented in this work, combined with complementary studies in the literature, establish a robust framework that guides experimentalists in exploring and validating the intriguing phenomena of dark solitons in optical fibers.

In summary, the experimental verification of dark solitons in optical fibers necessitates a comprehensive approach integrating pulse shaping techniques, nonlinear optical effects, and theoretical modeling. By harmonizing these methodologies, researchers can elucidate the fundamental properties and dynamics of dark solitons, advancing our understanding of nonlinear optics and optical communication technologies [49–54].

3.2. The Implementation of Extended Rational Cosh–Sinh Technique

Next, we choose the following form of solutions for Equations (9) and (10), as follows:

$$g(\eta) = \frac{p_0 \cosh(\mu\eta)}{p_2 + p_1 \sinh(\mu\eta)}, \quad (21)$$

where p_0 , p_1 , and p_2 are parameters that need to be established. Plugging Equation (21) into Equations (9) and (10), we collect the coefficients of $\sinh(\mu\eta)$ as follows:

$$\begin{aligned} \sinh^2(\mu\eta) &: p_1^2 r_1 + 2p_0^2 = 0, \\ \sinh^1(\mu\eta) &: 2r_1 - \mu^2 = 0, \\ \sinh^0(\mu\eta) &: 2\mu^2 p_1^2 + \mu^2 p_2^2 + p_2^2 r_1 + 2p_0^2 = 0, \end{aligned} \quad (22a)$$

&

$$\begin{aligned} \sinh^3(\mu\eta) &: p_1^2(\mu^2 - r_2) + 6p_0^2 = 0, \\ \sinh^2(\mu\eta) &: p_1^2(r_2 - 4\mu^2) - 2p_2^2(2\mu^2 + r_2) - 6p_0^2 = 0, \\ \sinh^1(\mu\eta) &: 2p_1^2(2\mu^2 + r_2) + p_2^2(\mu^2 - r_2) + 6p_0^2 = 0, \\ \sinh^0(\mu\eta) &: 2\mu^2 p_1(3p_1^2 + 2p_2^2) - p_1 p_2^2 r_2 + 6p_0^2 p_1 = 0. \end{aligned} \quad (22b)$$

By solving these algebraic sets in Equation (22), we determine the different sets of values p_0 , p_1 , p_2 , and μ given by the following:

Set 1:

$$\begin{aligned} c &= \frac{8\alpha_3^2 k^3 - 8\alpha_2 \alpha_3 k^2 + 2\alpha_2^2 k + 3\alpha_3 k v - \alpha_2 v}{\alpha_3}, \quad p_2 = \sqrt{-p_1} \sqrt{p_1}, \\ p_0 &= \pm \frac{p_1 \sqrt{3\alpha_3 k^2 - 2\alpha_2 k + v}}{\sqrt{2\alpha_3}}, \quad \mu = -\frac{\sqrt{2} \sqrt{-3\alpha_3 k^2 + 2\alpha_2 k - v}}{\sqrt{\alpha_3}}. \end{aligned} \quad (23)$$

Inserting these values into (8) with (21), we derive the following:

$$\psi(x, t) = \pm \left(\frac{\frac{p_1 \sqrt{3\alpha_3 k^2 - 2\alpha_2 k + v}}{\sqrt{2\alpha_3}} \cosh\left(-\frac{\sqrt{2} \sqrt{-3\alpha_3 k^2 + 2\alpha_2 k - v}}{\sqrt{\alpha_3}}(x - vt)\right)}{p_2 + p_1 \sinh\left(-\frac{\sqrt{2} \sqrt{-3\alpha_3 k^2 + 2\alpha_2 k - v}}{\sqrt{\alpha_3}}(x - vt)\right)} \right) \exp(i(kx - ct)). \quad (24)$$

Set 2:

$$\begin{aligned} c &= \frac{8\alpha_3^2 k^3 - 8\alpha_2 \alpha_3 k^2 + 2\alpha_2^2 k + 3\alpha_3 k v - \alpha_2 v}{\alpha_3}, \quad p_2 = -\sqrt{-p_1} \sqrt{p_1}, \\ p_0 &= \pm \frac{p_1 \sqrt{3\alpha_3 k^2 - 2\alpha_2 k + v}}{\sqrt{2\alpha_3}}, \quad \mu = -\frac{\sqrt{2} \sqrt{-3\alpha_3 k^2 + 2\alpha_2 k - v}}{\sqrt{\alpha_3}}. \end{aligned} \quad (25)$$

Substituting the above-obtained values into (8) along with (21), the associated soliton solution is determined by the following:

$$\psi(x, t) = \pm \left(\frac{\frac{p_1 \sqrt{3\alpha_3 k^2 - 2\alpha_2 k + v}}{\sqrt{2\alpha_3}} \cosh\left(-\frac{\sqrt{2} \sqrt{-3\alpha_3 k^2 + 2\alpha_2 k - v}}{\sqrt{\alpha_3}}(x - vt)\right)}{p_2 + p_1 \sinh\left(-\frac{\sqrt{2} \sqrt{-3\alpha_3 k^2 + 2\alpha_2 k - v}}{\sqrt{\alpha_3}}(x - vt)\right)} \right) \exp(i(kx - ct)). \quad (26)$$

Set 3:

$$c = \frac{8\alpha_3^2 k^3 - 8\alpha_2 \alpha_3 k^2 + 2\alpha_2^2 k + 3\alpha_3 k \nu - \alpha_2 \nu}{\alpha_3}, \quad p_2 = \sqrt{-p_1} \sqrt{p_1},$$

$$p_0 = \pm \frac{p_1 \sqrt{3\alpha_3 k^2 - 2\alpha_2 k + \nu}}{\sqrt{2\alpha_3}}, \quad \mu = -\frac{\sqrt{2} \sqrt{-3\alpha_3 k^2 + 2\alpha_2 k - \nu}}{\sqrt{\alpha_3}}. \quad (27)$$

Substituting these values into (8) with (21), the soliton solution is found by the following:

$$\psi(x, t) = \pm \left(\frac{\frac{p_1 \sqrt{3\alpha_3 k^2 - 2\alpha_2 k + \nu}}{\sqrt{2\alpha_3}} \cosh\left(-\frac{\sqrt{2} \sqrt{-3\alpha_3 k^2 + 2\alpha_2 k - \nu}}{\sqrt{\alpha_3}}(x - \nu t)\right)}{p_2 + p_1 \sinh\left(-\frac{\sqrt{2} \sqrt{-3\alpha_3 k^2 + 2\alpha_2 k - \nu}}{\sqrt{\alpha_3}}(x - \nu t)\right)} \right) \exp(i(kx - ct)). \quad (28)$$

Set 4:

$$c = \frac{8\alpha_3^2 k^3 - 8\alpha_2 \alpha_3 k^2 + 2\alpha_2^2 k + 3\alpha_3 k \nu - \alpha_2 \nu}{\alpha_3}, \quad p_2 = \sqrt{-p_1} \sqrt{p_1},$$

$$p_0 = \pm \frac{p_1 \sqrt{3\alpha_3 k^2 - 2\alpha_2 k + \nu}}{\sqrt{2\alpha_3}}, \quad \mu = \frac{\sqrt{2} \sqrt{-3\alpha_3 k^2 + 2\alpha_2 k - \nu}}{\sqrt{\alpha_3}}, \quad (29)$$

Plugging these set of values into (8) with (21), we obtain the following:

$$\psi(x, t) = \pm \left(\frac{\left(\frac{p_1 \sqrt{3\alpha_3 k^2 - 2\alpha_2 k + \nu}}{\sqrt{2\alpha_3}}\right) \cosh\left(\frac{\sqrt{2} \sqrt{-3\alpha_3 k^2 + 2\alpha_2 k - \nu}}{\sqrt{\alpha_3}}(x - \nu t)\right)}{p_2 + p_1 \sinh\left(\frac{\sqrt{2} \sqrt{-3\alpha_3 k^2 + 2\alpha_2 k - \nu}}{\sqrt{\alpha_3}}(x - \nu t)\right)} \right) \exp(i(kx - ct)). \quad (30)$$

The intensity profile of the singular soliton, described by solution (28), is generated through plotting. This profile is obtained with the following parameters: $p_1 = 0.5$, $\nu = 0.05$, $k = 0.005$, $\alpha_2 = 1$, and $\alpha_3 = 0.5$, as depicted in Figure 3a. For our convenience, we restrict the $|\psi|^2$ range to $[0, 250]$. In this representation, the singular soliton is observed to move toward the right side intensity as α_3 varies to 4, as shown in Figure 3b. Upon increasing the value of ν to 0.25, the profile of the singular soliton undergoes a notable transformation, transitioning into a periodically varying soliton structure. This shift is visualized in Figure 3c. Additionally, altering the value of k to 0.02 results in a rightward shift of the plane of the singular soliton, as illustrated in Figure 3d.

In Figure 4a, we explore the intriguing dynamics of singular solitons under the influence of varying α_3 , shedding light on their spatial movement. Initially, with $\alpha_3 = 0.25$ and $k = 0.005$, the singular soliton exhibits nuanced changes. Remarkably, as α_3 is increased to 2.5, the soliton's profile undergoes a perceptible shift, relocating from the central region towards the right side. Conversely, when α_3 is further increased to 4.5, the soliton profile experiences further displacement, illustrating the sensitivity of the soliton's behavior to variations in α_3 . Now, we vary the parameter k to analyze the spatial displacement phenomena in the singular soliton profiles. This outcome is depicted in Figure 4b. Expanding our investigation, Figure 4c explores the consequences of modifying ν on the singular soliton's characteristics. Enhancing ν from 0.06 to 0.15, we observe a remarkable change in the soliton's orientation. Moreover, this progression induces a transition towards a periodic structure in the soliton profile, showcasing the profound impact of parameter adjustments on the soliton's spatial dynamics. The periodicity increases with further increments in the value of ν . In essence, the findings depicted in Figure 4 unveil the intricate behavior of singular solitons, highlighting their sensitivity to variations in parameters such as α_3 , k , and ν . Such insights not only deepen our understanding of solitonic phenomena but also offer avenues for manipulating soliton characteristics in diverse physical systems.

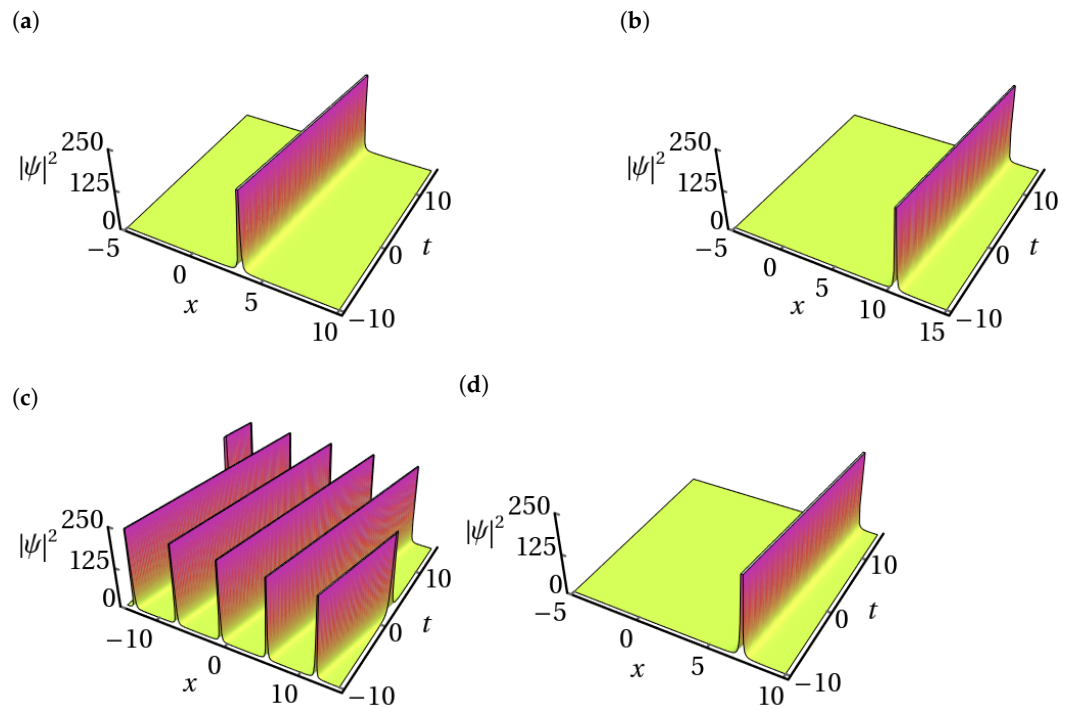


Figure 3. Intensity of singular soliton profiles for the third-order NLS Equation (7) using the solution (28). The parameters are (a) $p_1 = 0.5$, $\nu = 0.05$, $k = 0.005$, $\alpha_2 = 1$, $\alpha_3 = 0.5$; (b) $\alpha_3 = 4$; (c) $\nu = 0.25$; (d) $k = 0.02$. In (b–d), we vary the specified parameters while maintaining all other parameters at the same values as in (a).

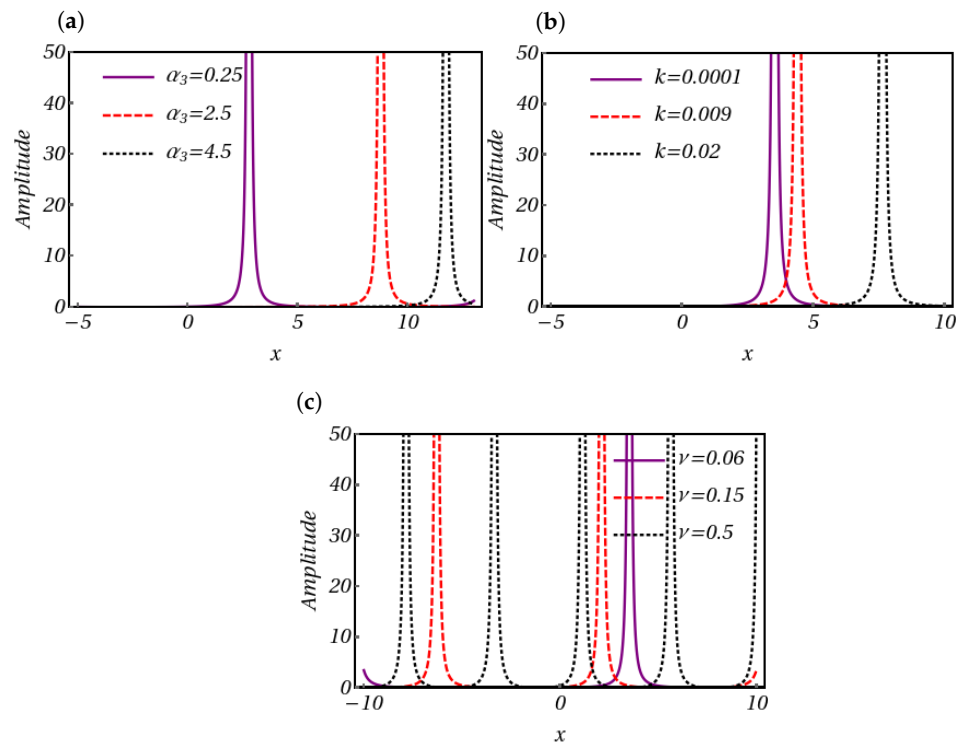


Figure 4. The variation in the profile of a singular soliton due to the influence of (a) α_3 with $k = 0.05 - 0.02i$, (b) α_3 with $k = 0.05 + 0.02i$, and (c) ν at $t = 0.01$. The other parameters are the same in Figure 3a.

3.3. The Implementation of the Extended Rational Sin–Cos Approach

In this section, we construct exact soliton solutions of the considered third-order NLS model (7) and explore their propagation as well as interaction dynamics in detail for different choices of parameters. To study this, we take into account the following forms of solutions for Equations (9) and (10):

$$g(\eta) = \frac{p_0 \sin(\mu\eta)}{p_2 + p_1 \cos(\mu\eta)}, \quad (31)$$

where p_0 , p_1 , and p_2 are parameters. Plugging Equation (31) into Equations (9) and (10), we collect the coefficients of $\cos(\mu\eta)$, as follows:

$$\begin{aligned} \cos^2(\mu\eta) : 2p_0^2 - p_1^2 r_1 &= 0, \\ \cos^1(\mu\eta) : \mu^2 + 2r_1 &= 0, \\ \cos^0(\mu\eta) : -\mu^2 p_2^2 + 2\mu^2 p_1^2 + p_2^2 r_1 + 2p_0^2 &= 0, \end{aligned} \quad (32a)$$

&

$$\begin{aligned} \cos^3(\mu\eta) : p_1^2(\mu^2 + r_2) + 6p_0^2 &= 0, \\ \cos^2(\mu\eta) : p_1^2(4\mu^2 + r_2) + 2p_2^2(r_2 - 2\mu^2) + 6p_0^2 &= 0, \\ \cos^1(\mu\eta) : 2p_1^2(r_2 - 2\mu^2) + p_2^2(\mu^2 + r_2) - 6p_0^2 &= 0, \\ \cos^0(\mu\eta) : 6\mu^2 p_1^2 - p_2^2(4\mu^2 + r_2) + 6p_0^2 &= 0. \end{aligned} \quad (32b)$$

By solving the algebraic Equation (32), the different sets of values p_0 , p_1 , p_2 , and μ are obtained. **Set 1:**

$$\begin{aligned} c &= \frac{8\alpha_3^2 k^3 - 8\alpha_2 \alpha_3 k^2 + 2\alpha_2^2 k + 3\alpha_3 k v - \alpha_2 v}{\alpha_3}, \quad p_2 = 0, \\ p_0 &= \pm \frac{\sqrt{-p_1} \sqrt{p_1} \sqrt{3\alpha_3 k^2 - 2\alpha_2 k + v}}{\sqrt{2\alpha_3}}, \quad \mu = -\frac{\sqrt{3\alpha_3 k^2 - 2\alpha_2 k + v}}{\sqrt{2\alpha_3}}. \end{aligned} \quad (33)$$

Plugging these sets of values into (8) along with (31), we obtain the following:

$$\psi(x, t) = \pm \left(\frac{\frac{\sqrt{-p_1} \sqrt{p_1} \sqrt{3\alpha_3 k^2 - 2\alpha_2 k + v}}{\sqrt{2\alpha_3}} \sin\left(-\frac{\sqrt{3\alpha_3 k^2 - 2\alpha_2 k + v}}{\sqrt{2\alpha_3}}(x - vt)\right)}{p_2 + p_1 \cos\left(-\frac{\sqrt{3\alpha_3 k^2 - 2\alpha_2 k + v}}{\sqrt{2\alpha_3}}(x - vt)\right)} \right) \exp(i(kx - ct)). \quad (34)$$

Set 2:

$$\begin{aligned} c &= \frac{8\alpha_3^2 k^3 - 8\alpha_2 \alpha_3 k^2 + 2\alpha_2^2 k + 3\alpha_3 k v - \alpha_2 v}{\alpha_3}, \quad p_2 = 0, \\ p_0 &= \pm \frac{\sqrt{-p_1} \sqrt{p_1} \sqrt{3\alpha_3 k^2 - 2\alpha_2 k + v}}{\sqrt{2\alpha_3}}, \quad \mu = \frac{\sqrt{3\alpha_3 k^2 - 2\alpha_2 k + v}}{\sqrt{2\alpha_3}}. \end{aligned} \quad (35)$$

Inserting the obtained values of c , p_0 , p_2 , and μ in Equation (8) with Equation (31), one can derive the following soliton solution:

$$\psi(x, t) = \pm \left(\frac{\frac{\sqrt{-p_1} \sqrt{p_1} \sqrt{3\alpha_3 k^2 - 2\alpha_2 k + v}}{\sqrt{2\alpha_3}} \sin\left(\frac{\sqrt{3\alpha_3 k^2 - 2\alpha_2 k + v}}{\sqrt{2\alpha_3}}(x - vt)\right)}{p_2 + p_1 \cos\left(\frac{\sqrt{3\alpha_3 k^2 - 2\alpha_2 k + v}}{\sqrt{2\alpha_3}}(x - vt)\right)} \right) \exp(i(kx - ct)). \quad (36)$$

Set 3:

$$c = \frac{8\alpha_3^2 k^3 - 8\alpha_2 \alpha_3 k^2 + 2\alpha_2^2 k + 3\alpha_3 k \nu - \alpha_2 \nu}{\alpha_3}, \quad p_2 = p_1,$$

$$p_0 = \pm \frac{\sqrt{-p_1} \sqrt{p_1} \sqrt{3\alpha_3 k^2 - 2\alpha_2 k + \nu}}{\sqrt{2\alpha_3}}, \quad \mu = -\frac{\sqrt{2} \sqrt{3\alpha_3 k^2 - 2\alpha_2 k + \nu}}{\sqrt{\alpha_3}}. \quad (37)$$

Substituting these forms into Equation (8) along with Equation (31), we acquire the following:

$$\psi(x, t) = \pm \left(\frac{\frac{\sqrt{-p_1} \sqrt{p_1} \sqrt{3\alpha_3 k^2 - 2\alpha_2 k + \nu}}{\sqrt{2\alpha_3}} \sin\left(-\frac{\sqrt{2} \sqrt{3\alpha_3 k^2 - 2\alpha_2 k + \nu}}{\sqrt{\alpha_3}} (x - \nu t)\right)}{p_2 + p_1 \cos\left(-\frac{\sqrt{2} \sqrt{3\alpha_3 k^2 - 2\alpha_2 k + \nu}}{\sqrt{\alpha_3}} (x - \nu t)\right)} \right) \exp(i(kx - ct)). \quad (38)$$

Set 4:

$$c = \frac{8\alpha_3^2 k^3 - 8\alpha_2 \alpha_3 k^2 + 2\alpha_2^2 k + 3\alpha_3 k \nu - \alpha_2 \nu}{\alpha_3}, \quad p_2 = p_1,$$

$$p_0 = \pm \frac{\sqrt{-p_1} \sqrt{p_1} \sqrt{3\alpha_3 k^2 - 2\alpha_2 k + \nu}}{\sqrt{2\alpha_3}}, \quad \mu = \frac{\sqrt{2} \sqrt{3\alpha_3 k^2 - 2\alpha_2 k + \nu}}{\sqrt{\alpha_3}}. \quad (39)$$

Plugging the above-obtained values into Equation (8) along with Equation (31), we obtain the following:

$$\psi(x, t) = \pm \left(\frac{\frac{\sqrt{-p_1} \sqrt{p_1} \sqrt{3\alpha_3 k^2 - 2\alpha_2 k + \nu}}{\sqrt{2\alpha_3}} \sin\left(\frac{\sqrt{2} \sqrt{3\alpha_3 k^2 - 2\alpha_2 k + \nu}}{\sqrt{\alpha_3}} (x - \nu t)\right)}{p_2 + p_1 \cos\left(\frac{\sqrt{2} \sqrt{3\alpha_3 k^2 - 2\alpha_2 k + \nu}}{\sqrt{\alpha_3}} (x - \nu t)\right)} \right) \exp(i(kx - ct)). \quad (40)$$

Utilizing the parameters $p_1 = 1$, $\nu = 0.01$, $k = 0.35$, $\alpha_2 = 1$, and $\alpha_3 = 0.1$, we generate an intensity profile corresponding to the dark soliton solution (34). This profile is visually represented in Figure 5a. Subsequently, as α_3 is adjusted to 0.5, a discernible shift occurs in the profile's characteristics: the amplitude decreases, accompanied by a slight increase in width, as depicted in Figure 5b. Continuing our exploration, we investigate the impact of altering the parameter ν , initially set at 0.01. As demonstrated in Figure 5c, when we increase ν to 0.45, we see a change in the direction of the dark soliton profile along with a decrease in amplitude. Furthermore, modifying the value of k to 0.85 leads to noteworthy changes in the dark soliton profile. Specifically, in Figure 5d, we witness an enhancement in the amplitude of the dark soliton profile, concomitant with a reduction in its width.

For different values of α_2 , a two-dimensional plot of the dark soliton profile is produced between its amplitude and x , as Figure 6a illustrates. The dark soliton profile amplitude diminishes and the profile width flattens at $\alpha_3 = 0.1$, 0.25, and 1.05. Figure 6b shows that the profile of dark soliton amplitude compresses as k increases (0.2, 0.7, and 1.5). Furthermore, extending the center region reduces the amplitude of the dark soliton form by increasing ν from 0.1 to 0.35, as seen in Figure 6c. Subsequently, by selecting $\nu = 0.7$, the dark soliton profile is transformed into a periodic form.

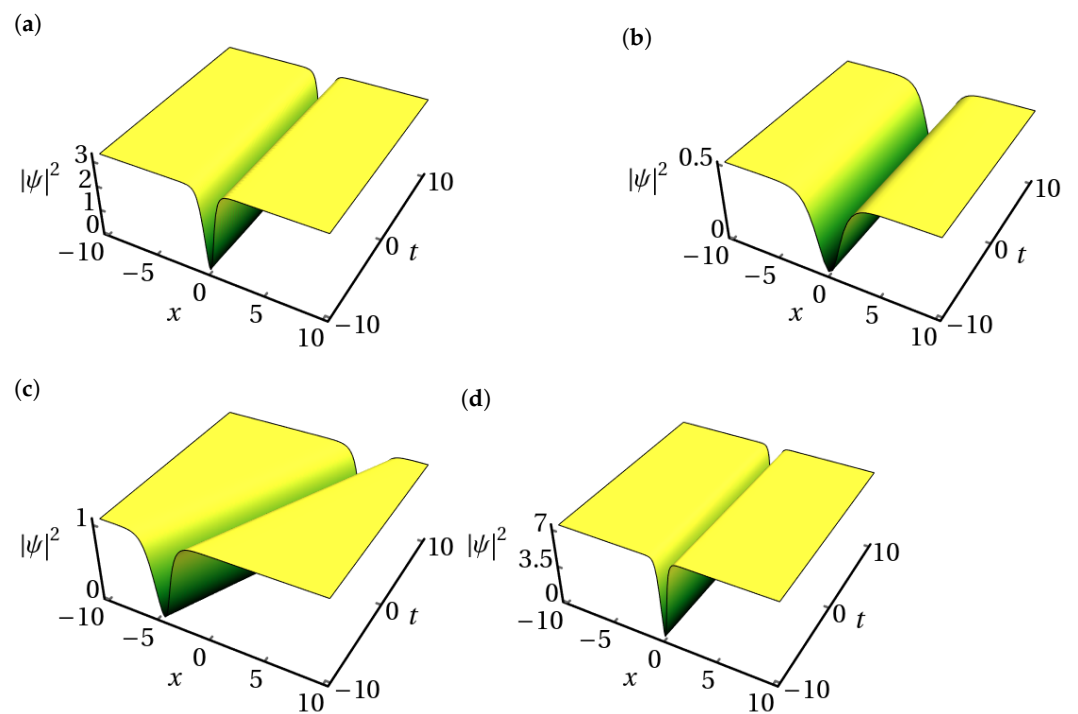


Figure 5. Intensity of dark soliton profiles for the third-order NLS Equation (7) using the solution (34). The parameters are (a) $p_1 = 1$, $\nu = 0.01$, $k = 0.35$, $\alpha_2 = 1$, $\alpha_3 = 0.1$; (b) $\alpha_3 = 0.5$; (c) $\nu = 0.45$; (d) $k = 0.85$. In (b–d), we vary the specified parameters while maintaining all other parameters at the same values as in (a).

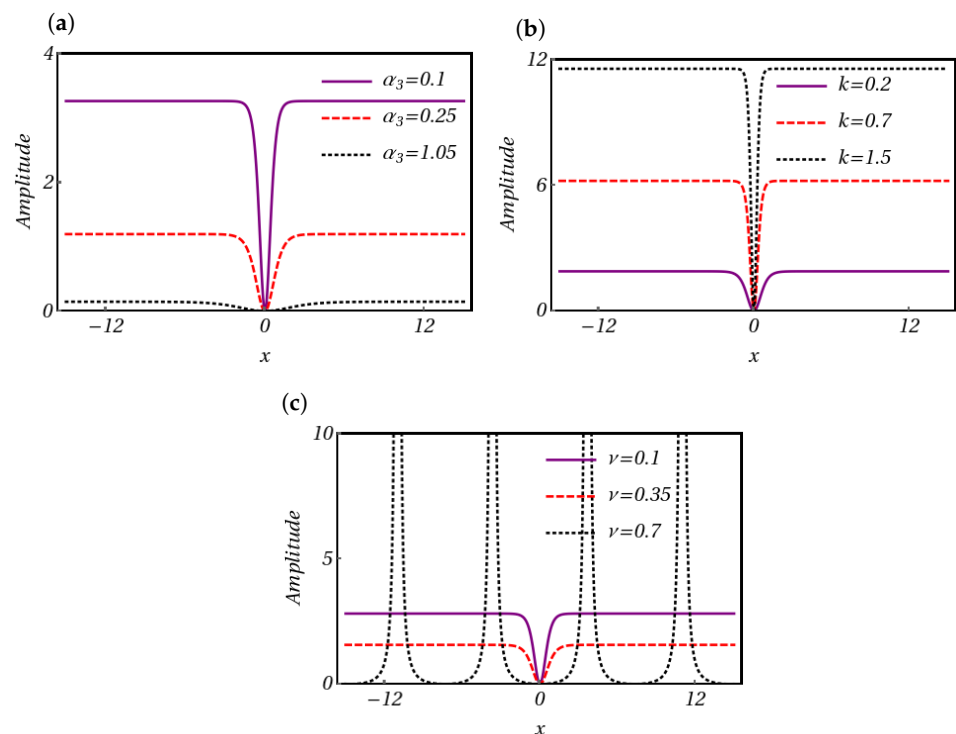


Figure 6. The magnitude variation in the amplitude of dark soliton due to the influence of (a) α_3 , (b) k , and (c) ν at $t = 0.01$. The other parameters are the same as in Figure 5a.

3.4. The Implementation of the Extended Rational Cos–Sin Approach

To investigate the dynamical features of singular solitons in the considered Equation (7), we adopt the solution for Equations (9) and (10) as follows:

$$g(\eta) = \frac{p_0 \cos(\mu\eta)}{p_2 + p_1 \sin(\mu\eta)}, \quad (41)$$

where p_0 , p_1 , and p_2 are parameters that are to be calculated. Plugging Equation (41) into Equations (9) and (10), we congregate the coefficients of $\sin(\mu\eta)$, namely the following:

$$\begin{aligned} \sin^2(\mu\eta) &: 2p_0^2 - p_1^2 r_1 = 0, \\ \sin^1(\mu\eta) &: \mu^2 + 2r_1 = 0, \\ \sin^0(\mu\eta) &: -\mu^2 p_2^2 + 2\mu^2 p_1^2 + p_2^2 r_1 + 2p_0^2 = 0, \end{aligned} \quad (42a)$$

&

$$\begin{aligned} \sin^3(\mu\eta) &: p_1^2(\mu^2 + r_2) + 6p_0^2 = 0, \\ \sin^2(\mu\eta) &: 2p_1^2(r_2 - 2\mu^2) + p_2^2(\mu^2 + r_2) - 6p_0^2 = 0, \\ \sin^1(\mu\eta) &: 2p_1^2(r_2 - 2\mu^2) + p_2^2(\mu^2 + r_2) - 6p_0^2 = 0, \\ \sin^0(\mu\eta) &: 6\mu^2 p_1^2 - p_2^2(4\mu^2 + r_2) + 6p_0^2 = 0. \end{aligned} \quad (42b)$$

By solving these algebraic system of Equations (42), one can deduce the different sets of values p_0 , p_1 , p_2 , and μ as follows:

Set 1:

$$\begin{aligned} c &= \frac{8\alpha_3^2 k^3 - 8\alpha_2 \alpha_3 k^2 + 2\alpha_2^2 k + 3\alpha_3 k v - \alpha_2 v}{\alpha_3}, \quad p_2 = 0, \\ p_0 &= \pm \frac{\sqrt{-p_1} \sqrt{p_1} \sqrt{3\alpha_3 k^2 - 2\alpha_2 k + v}}{\sqrt{2}\sqrt{\alpha_3}}, \quad \mu = -\frac{\sqrt{3\alpha_3 k^2 - 2\alpha_2 k + v}}{\sqrt{2}\sqrt{\alpha_3}}. \end{aligned} \quad (43)$$

We construct the following dark soliton solution by substituting the above-mentioned expression into Equation (8) along with the Equation (41), namely the following:

$$\psi(x, t) = \pm \left(\frac{\frac{\sqrt{-p_1} \sqrt{p_1} \sqrt{3\alpha_3 k^2 - 2\alpha_2 k + v}}{\sqrt{2}\alpha_3} \cos\left(-\frac{\sqrt{3\alpha_3 k^2 - 2\alpha_2 k + v}}{\sqrt{2}\alpha_3}(x - vt)\right)}{p_2 + p_1 \sin\left(-\frac{\sqrt{3\alpha_3 k^2 - 2\alpha_2 k + v}}{\sqrt{2}\alpha_3}(x - vt)\right)} \right) \exp(i(kx - ct)). \quad (44)$$

Set 2:

$$\begin{aligned} c &= \frac{8\alpha_3^2 k^3 - 8\alpha_2 \alpha_3 k^2 + 2\alpha_2^2 k + 3\alpha_3 k v - \alpha_2 v}{\alpha_3}, \quad p_2 = -p_1, \\ p_0 &= \pm \frac{\sqrt{-p_1} \sqrt{p_1} \sqrt{3\alpha_3 k^2 - 2\alpha_2 k + v}}{\sqrt{2}\alpha_3}, \quad \mu = \frac{\sqrt{2}\sqrt{3\alpha_3 k^2 - 2\alpha_2 k + v}}{\sqrt{\alpha_3}}. \end{aligned} \quad (45)$$

Inserting these forms in (8) along with Equation (41), we have the following:

$$\psi(x, t) = \pm \left(\frac{\frac{\sqrt{-p_1} \sqrt{p_1} \sqrt{3\alpha_3 k^2 - 2\alpha_2 k + v}}{\sqrt{2}\alpha_3} \cos\left(\frac{\sqrt{2}\sqrt{3\alpha_3 k^2 - 2\alpha_2 k + v}}{\sqrt{\alpha_3}}(x - vt)\right)}{p_2 + p_1 \sin\left(\frac{\sqrt{2}\sqrt{3\alpha_3 k^2 - 2\alpha_2 k + v}}{\sqrt{\alpha_3}}(x - vt)\right)} \right) \exp(i(kx - ct)). \quad (46)$$

Set 3:

$$c = \frac{8\alpha_3^2 k^3 - 8\alpha_2 \alpha_3 k^2 + 2\alpha_2^2 k + 3\alpha_3 k \nu - \alpha_2 \nu}{\alpha_3}, \quad p_2 = p_1,$$

$$p_0 = \pm \frac{\sqrt{-p_1} \sqrt{p_1} \sqrt{3\alpha_3 k^2 - 2\alpha_2 k + \nu}}{\sqrt{2\alpha_3}}, \quad \mu = -\frac{\sqrt{2} \sqrt{3\alpha_3 k^2 - 2\alpha_2 k + \nu}}{\sqrt{\alpha_3}}. \quad (47)$$

Plugging these expressions into Equation (8) with (41), one obtains the following soliton solution of (7):

$$\psi(x, t) = \pm \left(\frac{\frac{\sqrt{-p_1} \sqrt{p_1} \sqrt{3\alpha_3 k^2 - 2\alpha_2 k + \nu}}{\sqrt{2\alpha_3}} \cos\left(-\frac{\sqrt{2} \sqrt{3\alpha_3 k^2 - 2\alpha_2 k + \nu}}{\sqrt{\alpha_3}}(x - \nu t)\right)}{p_2 + p_1 \sin\left(-\frac{\sqrt{2} \sqrt{3\alpha_3 k^2 - 2\alpha_2 k + \nu}}{\sqrt{\alpha_3}}(x - \nu t)\right)} \right) \exp(i(kx - ct)). \quad (48)$$

Set 4:

$$c = \frac{8\alpha_3^2 k^3 - 8\alpha_2 \alpha_3 k^2 + 2\alpha_2^2 k + 3\alpha_3 k \nu - \alpha_2 \nu}{\alpha_3}, \quad p_2 = p_1,$$

$$p_0 = \pm \frac{\sqrt{-p_1} \sqrt{p_1} \sqrt{3\alpha_3 k^2 - 2\alpha_2 k + \nu}}{\sqrt{2} \sqrt{\alpha_3}}, \quad \mu = \frac{\sqrt{2} \sqrt{3\alpha_3 k^2 - 2\alpha_2 k + \nu}}{\sqrt{\alpha_3}}. \quad (49)$$

Substituting the above-mentioned forms in Equation (8) with (41), we obtain the following:

$$\psi(x, t) = \pm \left(\frac{\frac{\sqrt{-p_1} \sqrt{p_1} \sqrt{3\alpha_3 k^2 - 2\alpha_2 k + \nu}}{\sqrt{2\alpha_3}} \cos\left(\frac{\sqrt{2} \sqrt{3\alpha_3 k^2 - 2\alpha_2 k + \nu}}{\sqrt{\alpha_3}}(x - \nu t)\right)}{p_2 + p_1 \sin\left(\frac{\sqrt{2} \sqrt{3\alpha_3 k^2 - 2\alpha_2 k + \nu}}{\sqrt{\alpha_3}}(x - \nu t)\right)} \right) \exp(i(kx - ct)). \quad (50)$$

The singular soliton solution, characterized by spatial shift and periodicity, is described by the following parameters: $p_1 = 1$, $\nu = 0.01$, $k = 0.001$, $\alpha_2 = 1$, and $\alpha_3 = 0.1$. This solution is depicted using the solution (50), as demonstrated in Figure 7a. Upon varying the parameter α_3 to 1.25, depicted in Figure 7b, the singular soliton's profile shifts towards the left. In Figure 7c, it is observed that as the parameter ν is increased to 0.2, the profile of the singular soliton transforms into a periodically varying pattern. Additionally, modifying the parameter k to 0.0045 induces a spatial change in the profile, as illustrated in Figure 7d.

The two-dimensional representation of the singular soliton, with varying parameters α_3 , k , and ν , is illustrated in Figure 8. Further exploration involves manipulating α_3 to higher values, such as $\alpha_3 = 0.5$ and $\alpha_3 = 1.05$, resulting in a leftward shift of the soliton profile from its central position. This effect is visually depicted in Figure 8a. Increasing the values of k to 0.0001 and 0.004 causes a leftward shift of its profile from the center, as illustrated in Figure 8b. Further alterations are observed when adjusting the parameter ν , where increasing its value from 0.005 to 0.02, and subsequently to 0.25, leads to periodic changes in the singular soliton profile. Additionally, a periodic structure emerges in the profile with higher values of ν . These variations are represented in Figure 8c.

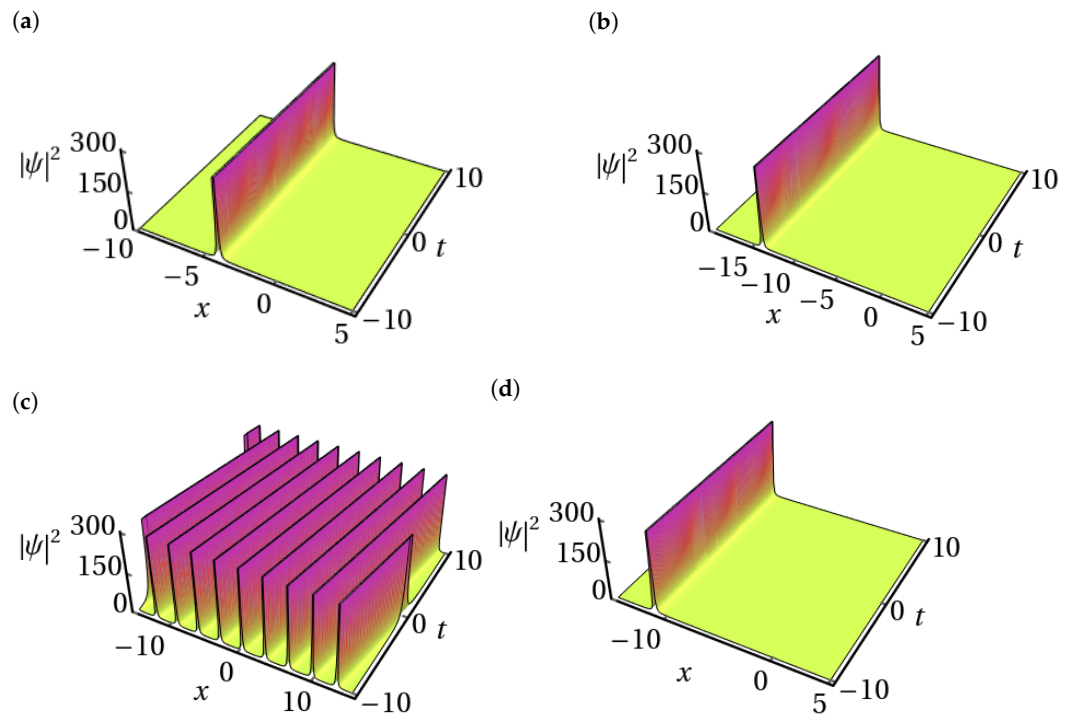


Figure 7. Intensity of singular soliton profiles for the third-order NLS Equation (7) using the solution (50). The parameters are (a) $p_1 = 1, \nu = 0.01, k = 0.001, \alpha_2 = 1, \alpha_3 = 0.1$; (b) $\alpha_3 = 1.25$; (c) $\nu = 0.2$; (d) $k = 0.0045$. In (b–d), we vary the specified parameters while maintaining all other parameters at the same values as in (a).

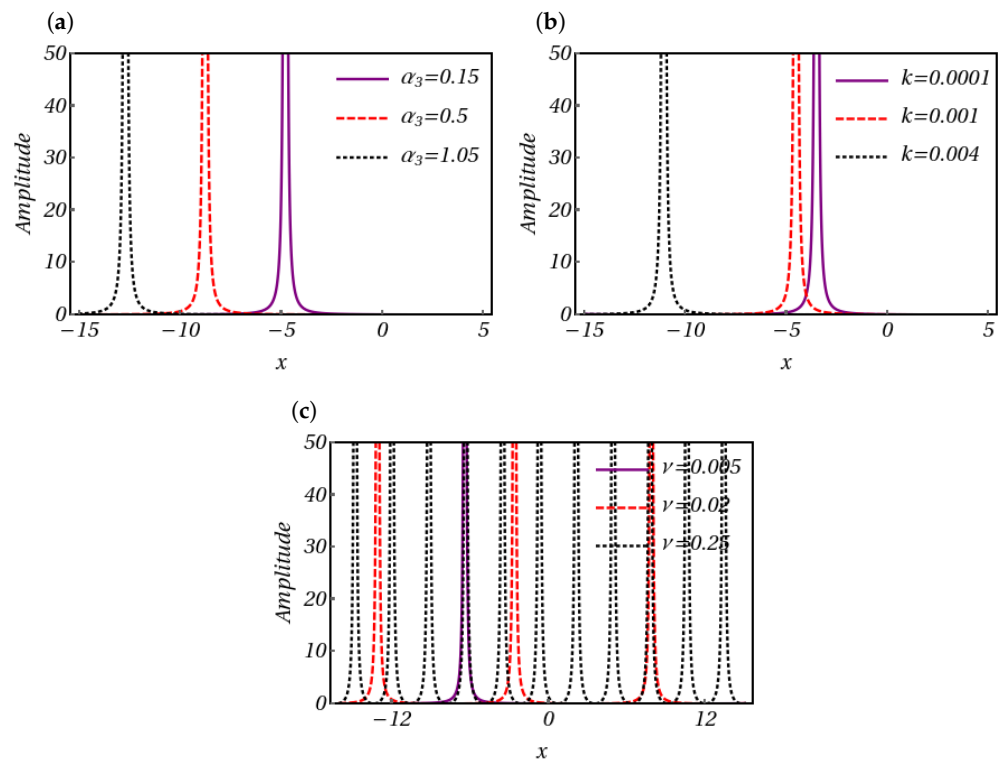


Figure 8. The variation in the profile of the singular soliton due to the influence of (a) α_3 , (b) k , and (c) ν at $t = 0.01$. The other parameters are the same as in Figure 7a.

4. Conclusions

In this work, we explored the third-order NLS equation, a pivotal model that elucidates the intricate dynamics governing the propagation of ultrashort pulses within optical fibers. We employed the extended rational sinh–cosh method and the extended rational sine–cosine method to derive exact solutions, encompassing both dark and singular solitons, for the third-order NLS equation. These methods, noted for their efficacy and widespread applicability, are instrumental in constructing solutions that offer profound insights into the dynamics of optical pulse propagation. Through our investigations, we unveil a plethora of new exact traveling wave solutions, characterized by expressions involving hyperbolic functions, trigonometric functions, and complex functions. These solutions not only contribute to the theoretical understanding of nonlinear wave phenomena but also hold practical significance in optical fiber communication systems. Furthermore, by carefully selecting specific parameter values, we visualize the physical structures corresponding to these solutions, elucidating their intrinsic nature and characteristics. Notably, our observations reveal intriguing behaviors: the intensity of soliton profiles escalates with variations in the parameter k , while adjustments to the parameters ν and α_3 lead to a decrease in soliton intensity profiles. These findings provide valuable insights into the controllability and manipulation of soliton dynamics in optical fiber systems, with implications for a wide range of applications in nonlinear optics and photonics.

Author Contributions: Conceptualization, K.M.; methodology, A.M., K.M. and N.S.; software, A.M. and A.S.; validation, N.S.; formal analysis, A.S. and N.S.; investigation, K.M.; writing—original draft, K.M.; writing—review and editing, A.M. and N.S.; visualization, A.S. All authors have read and agreed to the published version of the manuscript.

Funding: This research received no external funding.

Data Availability Statement: No data was used for the research described in the article.

Acknowledgments: A.M. and K.M. gratefully acknowledge the Center for Computational Modeling, Chennai Institute of Technology, India, funding number CIT/CCM/2024/RP-012. K.M. is also supported by the Science and Engineering Research Board (SERB), Govt. of India, through MATRICS research (grant no. MTR/2023/000921). This work is also supported by the Ministry of Science and Higher Education of the Republic of Kazakhstan, grant no. AP19675202.

Conflicts of Interest: The authors declare no conflicts of interest.

References

1. Kivshar, Y.S.; Agrawal, G.P. *Optical Solitons: From Fibers to Photonic Crystals*; Academic Press: San Diego, CA, USA, 2003.
2. Porsezian, K.; Kuriakose, V.C. *Optical Solitons: Theoretical and Experimental Challenges*; Springer: New York, NY, USA, 2003.
3. Dudley, J.M.; Finot, C.; Genty, G.; Taylor, R. Fifty years of fiber solitons. *Opt. Photon. News* **2023**, *34*, 26. [[CrossRef](#)]
4. Kibler, B.; Fatome, J.; Finot, C.; Millot, G.; Dias, F.; Genty, G.; Akhmediev, N.; Dudley, J.M. The Peregrine soliton in nonlinear fibre optics. *Nat. Phys.* **2010**, *6*, 790. [[CrossRef](#)]
5. Lakshmanan, M.; Rajasekar, S. *Nonlinear Dynamics: Integrability, Chaos and Patterns*; Springer: Berlin/Heidelberg, Germany, 2003.
6. Musammil, N.M.; Porsezian, K.; Nithyanandan, K.; Subha, P.A.; Tchofo Dinda, P. Ultrashort dark solitons interactions and nonlinear tunneling in the modified nonlinear Schrödinger equation with variable coefficient. *Opt. Fiber Technol.* **2017**, *37*, 11–20. [[CrossRef](#)]
7. Tahir, M.; Awan, A.U. Optical dark and singular solitons to the Biswas-Arshed equation in birefringent fibers without four-wave mixing. *Optik* **2020**, *207*, 164421. [[CrossRef](#)]
8. Zhang, H.; Tang, D.Y.; Zhao, L.M.; Wu, X. Dark pulse emission of a fiber laser. *Phys. Rev. A* **2009**, *80*, 045803. [[CrossRef](#)]
9. Kevrekidis, P.G.; Frantzeskakis, D.J.; Carretero-González, R. *Emergent Nonlinear Phenomena in Bose-Einstein Condensates: Theory and Experiment*; Springer: Berlin/Heidelberg, Germany, 2008.
10. Hasegawa, A.; Tappert, F.D. Transmission of stationary nonlinear optical pulses in dispersive dielectric fibers. I. Anomalous dispersion. *Appl. Phys. Lett.* **1973**, *23*, 142. [[CrossRef](#)]
11. Zakharov, V.; Shabat, A. Exact theory of two dimensional self-focusing and one dimensional self-modulation of waves in nonlinear media. *Sov. Phys. JETP* **1972**, *34*, 62.
12. Emplit, P.; Hamaide, J.P.; Reynaud, F.; Froehly, C.; Barthelemy, A. Picosecond steps and dark pulses through nonlinear single mode fibers. *Opt. Commun.* **1987**, *62*, 374. [[CrossRef](#)]

13. Liu, W.; Pang, L.; Han, H.; Tian, W.; Chen, H.; Lei, M.; Yan, P.; Wei, Z. Generation of dark solitons in erbium-doped fiber lasers based Sb_2Te_3 saturable absorbers. *Opt. Express* **2015**, *23*, 26023–26031. [[CrossRef](#)]
14. Zhang, H.; Tang, D.Y.; Zhao, L.M.; Knize, R.J. Vector dark domain wall solitons in a fiber ring laser. *Opt. Express* **2010**, *18*, 4428–4433. [[CrossRef](#)]
15. Meng, Y.; Zhang, S.; Li, H.; Du, J.; Hao, Y.; Li, X. Bright-dark soliton pairs in a self-mode locking fiber laser. *Opt. Eng.* **2012**, *51*, 064302. [[CrossRef](#)]
16. Tang, D.Y.; Li, L.; Song, Y.F.; Zhao, L.M.; Zhang, H.; Shen, D.Y. Evidence of dark solitons in all-normal-dispersion-fiber lasers. *Phys. Rev. A* **2013**, *88*, 013849. [[CrossRef](#)]
17. Tang, D.; Guo, J.; Song, Y.; Zhang, H.; Zhao, L.; Shen, D. Dark soliton fiber lasers. *Opt. Express* **2014**, *22*, 19831–19837. [[CrossRef](#)] [[PubMed](#)]
18. Rajan, M.; Hakkim, J.; Mahalingam, A.; Uthayakumar, A. Dispersion management and cascade compression of femtosecond nonautonomous soliton in birefringent fiber. *Eur. Phys. J. D* **2013**, *67*, 1–8. [[CrossRef](#)]
19. Mahalingam, A.; Rajan, M.M. Influence of generalized external potentials on nonlinear tunneling of nonautonomous solitons: Soliton management. *Opt. Fib. Technol.* **2015**, *25*, 44–50. [[CrossRef](#)]
20. Pelinovsky, D.E.; Yang, J. Stability analysis of embedded solitons in the generalized third-order nonlinear Schrödinger equation. *Chaos* **2005**, *15*, 037115. [[CrossRef](#)] [[PubMed](#)]
21. Hosseini, K.; Osman, M.S.; Mirzazadeh, M.; Rabiei, F. Investigation of different wave structures to the generalized third-order nonlinear Schrödinger equation. *Optik* **2020**, *206*, 164259. [[CrossRef](#)]
22. Crabb, M.; Akhmediev, N. Doubly periodic solutions of the class-I infinitely extended nonlinear Schrödinger equation. *Phys. Rev. E* **2019**, *99*, 052217. [[CrossRef](#)] [[PubMed](#)]
23. Sinthuja, N.; Manikandan, K.; Senthilvelan, M. Rogue waves on the double-periodic background in Hirota equation. *Eur. Phys. J. Plus* **2021**, *136*, 1–12. [[CrossRef](#)]
24. Malomed, B.A.; Mihalache, D. Nonlinear waves in optical and matter-wave media: A topical survey of recent theoretical and experimental results. *Rom. J. Phys.* **2019**, *64*, 106.
25. Mihalache, D.; Truta, N.; Crasovan, L.C. Painleve analysis and bright solitary waves of the higher-order nonlinear Schrödinger equation containing third-order dispersion and self-steepening term. *Phys. Rev. E* **1997**, *56*, 1064–1070. [[CrossRef](#)]
26. Zhang, H.Q.; Yuan, S.S. Dark soliton solutions of the defocusing Hirota equation by the binary Darboux transformation. *Nonlinear Dyn.* **2017**, *89*, 531–538. [[CrossRef](#)]
27. Shaikhova, G.; Kutum, B.; Myrzakulov, R. Periodic traveling wave, bright and dark soliton solutions of the (2+1)-dimensional complex modified Korteweg-de Vries system of equations by using three different methods. *AIMS Math.* **2022**, *7*, 18948–18970. [[CrossRef](#)]
28. Myrzakul, A.; Nugmanova, G.; Serikbayev, N.; Myrzakulov, R. Surfaces and curves induced by nonlinear Schrödinger-type equations and their spin systems. *Symmetry* **2021**, *13*, 1827. [[CrossRef](#)]
29. Sagidullayeva, Z.; Nugmanova, G.; Myrzakulov, R.; Serikbayev, N. Integrable Kuralay equations: Geometry, solutions and generalizations. *Symmetry* **2022**, *14*, 1374. [[CrossRef](#)]
30. Burdik, C.; Shaikhova, G.; Rakhimzhanov, B. Soliton solutions and traveling wave solutions of the two-dimensional generalized nonlinear Schrödinger equations. *Eur. Phys. J. Plus* **2021**, *136*, 1095. [[CrossRef](#)]
31. Zhang, S.; Zhu, F.; Xu, B. Localized Symmetric and Asymmetric Solitary Wave Solutions of Fractional Coupled Nonlinear Schrödinger Equations. *Symmetry* **2023**, *15*, 1211. [[CrossRef](#)]
32. Manikandan, K.; Serikbayev, N.; Vijayasree, S.P.; Aravinthan, D. Controlling Matter-Wave Smooth Positons in Bose–Einstein Condensates. *Symmetry* **2023**, *15*, 1585. [[CrossRef](#)]
33. Shaikhova, G.; Kutum, B.; Syzdykova, A. Phase portraits and new exact traveling wave solutions of the (2+1)-dimensional Hirota system. *Results Phys.* **2023**, *55*, 107173. [[CrossRef](#)]
34. Gerdjikov, V.S.; Stefanov, A.A. Riemann–Hilbert Problems, Polynomial Lax Pairs, Integrable Equations and Their Soliton Solutions. *Symmetry* **2023**, *15*, 1933. [[CrossRef](#)]
35. Hirota, R. *The Direct Method in Soliton Theory*; Cambridge University Press: Cambridge, UK, 2004.
36. Seadawy, A.R.; El-Rashidy, K. Application of the extension exponential rational function method for higher-dimensional Broer–Kaup–Kupershmidt dynamical system. *Mod. Phys. Lett. A* **2020**, *35*, 1950345. [[CrossRef](#)]
37. Zayed, E.M.E.; Alurffi, K.A.E. A new Jacobi elliptic function expansion method for solving a nonlinear PDE describing the nonlinear low-pass electrical lines. *Chaos Solitons Fractals* **2015**, *78*, 148–155. [[CrossRef](#)]
38. Zeković, S.; Muniyappan, A.; Zdravković, S.; Kavitha, L. Employment of Jacobian elliptic functions for solving problems in nonlinear dynamics of microtubules. *Chin. Phys. B* **2014**, *23*, 020504. [[CrossRef](#)]
39. Biswas, A.; Alqahtani, R.T. Chirp-free bright optical solitons for perturbed Gerdjikov–Ivanov equation by semi-inverse variational principle. *Optik* **2017**, *147*, 72–76. [[CrossRef](#)]
40. Muniyappan, A.; Suruthi, A.; Monisha, B.; Sharon Leela, N.; Vijaycharles, J. Dromion-like structures in a cubic-quintic nonlinear Schrödinger equation using analytical methods. *Nonlinear Dyn.* **2021**, *104*, 1533–1544. [[CrossRef](#)]
41. Qayyum, M.; Ahmad, E.; Tauseef Saeed, S.; Ahmad, H.; Askar, S. Homotopy perturbation method-based soliton solutions of the time-fractional (2+1)-dimensional Wu–Zhang system describing long dispersive gravity water waves in the ocean. *Front. Phys.* **2023**, *11*, 1178154. [[CrossRef](#)]

42. Mahak, N.; Akram, G. Extension of rational sine-cosine and rational sinh-cosh techniques to extract solutions for the perturbed NLSE with Kerr law nonlinearity. *Eur. Phys. J. Plus* **2019**, *134*, 159. [[CrossRef](#)]
43. Muniyappan, A.; Parasuraman, E.; Seadawy, A.R.; Sudharsan, J.B. Chirped dark soliton propagation in optical fiber under a self phase modulation and a self-steepening effect for higher order nonlinear Schrödinger equation. *Opt. Quant. Electron.* **2024**, *56*, 772. [[CrossRef](#)]
44. Cinar, M.; Onder, I.; Secer, A.; Yusuf, A.; Sulaiman, T.A.; Bayram, M.; Aydin, H. The analytical solutions of Zoomeron equation via extended rational sin-cos and sinh-cosh methods. *Phys. Scr.* **2021**, *96*, 094002. [[CrossRef](#)]
45. Karchi, N.A.; Ghaemi, M.B.; Vahidi, J. New exact solutions of nonlinear Schrödinger equation with extended rational sin-cos and sinh-cosh method. *AIP Adv.* **2022**, *12*, 085110. [[CrossRef](#)]
46. Ankiewicz, A.; Soto-Crespo, J.M.; Akhmediev, N. Rogue waves and rational solutions of the Hirota equation. *Phys. Rev. E* **2010**, *81*, 046602. [[CrossRef](#)] [[PubMed](#)]
47. Shi, K.Z.; Ren, B.; Shen, S.F.; Wang, G.F.; Peng, J.D.; Wang, W.L. Solitons, rogue waves and interaction behaviors of a third-order nonlinear Schrödinger equation. *Results Phys.* **2022**, *37*, 105533. [[CrossRef](#)]
48. Tao, Y.S.; He, J.S. Multisolitons, breathers, and rogue waves for the Hirota equation generated by the Darboux transformation. *Phys. Rev. E* **2012**, *85*, 026601. [[CrossRef](#)] [[PubMed](#)]
49. Yang, S.; Zhang, Q.Y.; Zhu, Z.W.; Qi, Y.Y.; Yin, P.; Ge, Y.Q.; Li, L.; Jin, L.; Zhang, L.; Zhang, H. Recent advances and challenges on dark solitons in fiber lasers. *Opt. Laser Technol.* **2022**, *152*, 108116. [[CrossRef](#)]
50. Ablowitz, M.J.; Nixon, S.D.; Horikis, T.P.; Frantzeskakis, D.J. Dark solitons of the power-energy saturation model: Application to mode-locked lasers. *J. Phys. A Math. Theor.* **2013**, *46*, 095201. [[CrossRef](#)]
51. Yang, S.; Zhang, Q.Y.; Li, L.; Jin, L.; Chen, S. Generation of Dark Solitons in a Self-mode-locked Tm-Ho Doped Fiber Laser. *Infrared Phys. Technol.* **2022**, *121*, 104043. [[CrossRef](#)]
52. Weiner, A.M.; Heritage, J.P.; Hawkins, R.J.; Thurston, R.N.; Kirschner, E.M. Experimental Observation of the Fundamental Dark Soliton in Optical Fibers. *Phys. Rev. Lett.* **1988**, *61*, 2445–2448. [[CrossRef](#)] [[PubMed](#)]
53. Emplit, P.H.; Haelterman, M.; Kashyap, R.; De Lathouwer, M. Fiber Bragg grating for optical dark soliton generation. *IEEE Photonics Technol. Lett.* **1997**, *9*, 1122–1124. [[CrossRef](#)]
54. Li, H.P.; Xia, H.D.; Jing, Z.; Liao, J.K.; Tang, X.G.; Liu, Y.; Liu, Y.Z. Dark pulse generation in a dispersion-managed fiber laser. *Laser Phys.* **2012**, *22*, 261–264. [[CrossRef](#)]

Disclaimer/Publisher's Note: The statements, opinions and data contained in all publications are solely those of the individual author(s) and contributor(s) and not of MDPI and/or the editor(s). MDPI and/or the editor(s) disclaim responsibility for any injury to people or property resulting from any ideas, methods, instructions or products referred to in the content.